nature sustainability

Analysis

https://doi.org/10.1038/s41893-024-01291-0

Wildfire risk for global wildland–urban interface areas

Received: 9 October 2022

Accepted: 23 January 2024

Published online: 26 February 2024

Check for updates

Bin Chen[1,2,3] ✉, Shengbiao Wu[1], Yufang Jin[4], Yimeng Song[5], Chao Wu[6,7], Sergey Venevsky[8,9], Bing Xu[8], Chris Webster[2,3,10] & Peng Gong[2,11]

Intensifying wildfires and human settlement expansion have placed more people and infrastructure at the wildland–urban interface (WUI) areas under risk. Effective wildfire management and policy response are needed to protect ecosystems and residential communities; however, maps containing spatially and temporally explicit information on the distribution of WUI areas are limited to certain countries or local regions, and global WUI patterns and associated wildfire exposure risk therefore remain unclear. Here we generated the global WUI data layers for the 2020 baseline and the 1985–2020 time series by integrating fine-resolution housing and vegetation mapping. We estimated the total global WUI area to be 6.62 million km^2. Time-series analysis revealed that global WUI areas increased by 12.56% between 1985 and 2020. By overlapping 2001–2020 wildfire burned area maps and fine-resolution population datasets, our analysis uncovered that globally, 7.07% (12.54%) of WUI areas housing 4.47 million (10.11 million) people are within a 2,400 m (4,800 m) buffer zone of wildfire threat. Regionally, we found that the United States, Brazil, China, India and Australia account for the majority of WUI areas, but African countries experience higher wildfire risk. Our quantification of global WUI spatiotemporal patterns and the associated wildfire risk could support improvement of wildfire management.

Wildfires significantly influence the characteristics of ecosystems[1] and have widespread impacts on the environment, wildlife, human health and infrastructure[2–5]. Recent years have brought more record-breaking wildfire activities worldwide, from Australia to the Arctic, spanning Europe, North America and South America[6]. These wildfires have consumed vast areas of vegetation, threatened communities, caused severe air pollution and escalated firefighting costs[7,8]. The media's coverage of catastrophic wildfires has garnered global attention, highlighting the urgent need to mitigate wildfire risk as more critical than ever.

[1]Future Urbanity & Sustainable Environment (FUSE) Lab, Division of Landscape Architecture, Department of Architecture, Faculty of Architecture, The University of Hong Kong, Hong Kong SAR, China. [2]Urban Systems Institute and Institute for Climate and Carbon Neutrality, The University of Hong Kong, Hong Kong SAR, China. [3]Musketeers Foundation Institute of Data Science, The University of Hong Kong, Hong Kong SAR, China. [4]Department of Land, Air and Water Resources, University of California, Davis, Davis, CA, USA. [5]School of the Environment, Yale University, New Haven, CT, USA. [6]Wilkes Center for Climate Science and Policy, University of Utah, Salt Lake City, UT, USA. [7]School of Biological Sciences, University of Utah, Salt Lake City, UT, USA. [8]Department of Earth System Science, Ministry of Education Ecological Field Station for East Asian Migratory Birds, and Institute for Global Change Studies, Tsinghua University, Beijing, China. [9]Southern Scientific Centre of RAS, Rostov-on-Don, Russia. [10]HKUrbanLabs, Faculty of Architecture, The University of Hong Kong, Hong Kong SAR, China. [11]Department of Geography and Department of Earth Sciences, The University of Hong Kong, Hong Kong SAR, China. ✉e-mail: binley.chen@hku.hk

Climate plays a pivotal role in shaping wildfire activities, regulating the interplay among ignition sources, vegetation growth, fuel moisture and meteorological conditions[9]. Factors such as rising temperature[10–12], increasing atmospheric aridity[8,13], decreased precipitation[14] and prevalent droughts[15,16] have been linked to the heightened intensity of wildfire regimes from regional to global scales. Beyond natural causes, human activities and land-use changes have further amplified wildfire risk[8,9,17–19]. Specifically, the rapid expansion of human settlements in wilderness regions, referred to as the wildland–urban interface (WUI)[20], has placed more people at the nexus of natural vegetation and populated areas. This expansion has also improved access to easily combustible fuels due to road development. Moreover, the proliferation of electrical infrastructure and transmission lines, coupled with WUI development, adds to the wildfire risk, especially during extreme weather events such as lightning storms, severe heatwaves and strong wind gusts[3,17]. Over the past few decades, the WUI, which is characterized by housing and structures built close to or within natural vegetation, has emerged as a central concern in wildfire policy and management globally, with particular exposure in the United States[18,20–23], Canada[24], Australia[25] and many European countries[26,27]. It is deduced, both logically and empirically, that the WUI emerges as the planetary zone where wildfires pose the greatest risk to people due to the proximity of flammable vegetation[18,20,28]. As a result, efforts to map the WUI with the objective of quantifying the spatial extent and temporal evolution in areas vulnerable to wildfire risk have received considerable attention among the researchers and forest management bodies.

While there is an increasing amount of research focused on WUI mapping[28,29], a comprehensive and accurate dataset detailing global WUI areas and their historical evolutions is lacking. More importantly, the variation in exposure to wildfire risk in different WUI areas remains unclear. For a reliable comparison between different regions and countries, it is essential that the quantification of the WUI area and the associated wildfire risk should be derived from the same or compatible data sources, mapping and assessment methods. As we look ahead, standardizing data, risk assessment methodologies, legal frameworks and so on will become particularly vital in the future, as the global insurance industry partners with governments to navigate the complex matter of insuring properties and individuals against wildfire threats[30].

To tackle these challenges, we generated a global WUI map based on fine-resolution housing and vegetation mapping from 2020 satellite sources. We also produced a long-term time series of global WUI maps tracing consistent land cover and human settlement patterns from 1985 to 2020. The mapping endeavours were designed to elucidate the spatiotemporal patterns of global WUIs and help assess the relative risk of wildfire globally (Supplementary Fig. 1). Our study specifically addresses the following four questions. (1) What is the spatial pattern of WUI areas globally? (2) How have global WUI areas evolved over the past few decades? (3) What are the differences in wildfire risk among WUI areas? (4) To what extent is the global population exposed to wildfire risk in WUI areas?

Results

Mapping the WUI

The WUI areas identified in this study are shown in Fig. 1. Specifically, what we classify as interface WUIs, which are by definition located near large areas of dense wildland vegetation[18] (Methods), typically appear as buffer shapes, either polygons or polylines (Fig. 1b). These highlight the narrow interface between dense human settlements and wildland vegetation (as illustrated in Fig. 1b). Conversely, intermix WUIs, where housing and wildland vegetation intermingle, are either more dispersed or more isolated spatially (Fig. 1b). This primarily hinges the spatial layout of rural human dwellings (as illustrated in Fig. 1b).

When compared with the most frequently used WUI map of the conterminous United States (from the SILVIS lab[18]) (Supplementary Fig. 2), the fine-scale WUI map generated in our present study shows similar patterns in the overall WUI distribution. The majority of WUI areas are clustered in the central and eastern United States. Nevertheless, our map excels in capturing the granular spatial details of WUI distribution by accounting for individual house footprints, as exemplified in the depiction of California (Supplementary Fig. 2). At the state level, both products are consistent ($R^2 = 0.72$) (Supplementary Fig. 3); however, our approach identified more WUI areas, extending by an additional 0.35 million km^2, and successfully tracked the expansion of the total WUI area during 2010–2020. Moreover, when compared with the recently released WUI map at the global scale[29], the state-level comparison achieved a very high consistency with R^2 of 0.90 (Supplementary Fig. 4).

Global WUI patterns

We estimate that the total global area of WUI is 6.62 million km^2 (Table 1). At the continent level, Asia takes the lead with a total area of WUI covering 1.79 million km^2, followed by North America with 1.41 million km^2 and Europe with 1.25 million km^2. Europe has the highest areal proportion of WUI, accounting for 13.00% of its total land area, followed by South America at 5.21% and North America at 5.17%. The intermix type is the dominant WUI globally and makes up 76.2% of the total (5.04 million km^2), while interface WUI accounts for the remaining 23.8% (1.58 million km^2). We also found that the proportion between interface and intermix WUIs varies across continents, as shown in the global map and the insets of Fig. 1. Asia and Europe show much higher proportions of interface WUI (that is, 34.4% and 24.6%, respectively) (Table 1); the proportions in Africa (21.0%) and North America (18.9%) are close to the global level of 23.8%, while intermix WUI is dominant in South America (86.0%) and Australia/Oceania (87.0%).

Diving deeper into the map, we aggregated total WUI area across the widely used Global Fire Emissions Database (GFED) fire regions (Supplementary Fig. 5) and two administrative scales to report the global pattern of WUI distribution across GFED regions, countries (Fig. 2a) and states (Fig. 2b). Analysing by GFED world regions (Supplementary Table 1), the results show that Temperate North America, Europe and Southeast Asia have relatively larger WUI areas, covering 1.12 million km^2 (approximately 13.98% of its total land), 1.02 million km^2 (approximately 13.22% of its total land) and 0.79 million km^2 (approximately 11.12% of its total land), respectively. At the country level, the top ten countries with the largest area of WUI are the United States (1.12 million km^2), Brazil (0.48 million km^2), India (0.37 million km^2), China (0.35 million km^2), Indonesia (0.21 million km^2), France (0.18 million km^2), Russia (0.15 million km^2), Mexico (0.13 million km^2), Germany (0.11 million km^2) and Ethiopia (0.11 million km^2) (Fig. 2a).

At the state level, we found a more clustered distribution of WUIs. For example, in the United States, a substantial proportion of WUI areas are distributed in central and eastern states such as Texas (89,122 km^2), North Carolina (49,630 km^2), Pennsylvania (48,683 km^2), Missouri (48,562 km^2) and Michigan (44,735 km^2). However, the western side of the United States, especially California (31,743 km^2) and Washington (17,999 km^2), also has significant WUI areas. In Brazil, the majority of WUI areas are found in Minas Gerais (76,518 km^2), Bahia (42,318 km^2), Sao Paulo (38,793 km^2), Rio Grande do Sul (36,859 km^2) and Parana (29,527 km^2). These five states collectively account for nearly half (46.7%) of Brazil's total WUI area. In Africa, states such as Oromia in Ethiopia (44,268 km^2); the Rift Valley of Kenya (28,671 km^2); the Southern Nations, Nationalities, and People's Region of Ethiopia (25,701 km^2); KwaZulu-Natal of South Africa (23,918 km^2); and parts of eastern Kenya (21,795 km^2) emerge as WUI-dense zones. Asian WUI focal points are predominantly distributed in regions of southern China and India (Fig. 2b). In Australia, New South Wales stands out with a much larger WUI area (32,211 km^2) than its counterparts. The spatial distributions of interface and intermix WUIs, at both the country and state levels, are further illustrated in Supplementary Figs. 6 and 7.

https://doi.org/10.1038/s41893-024-01291-0

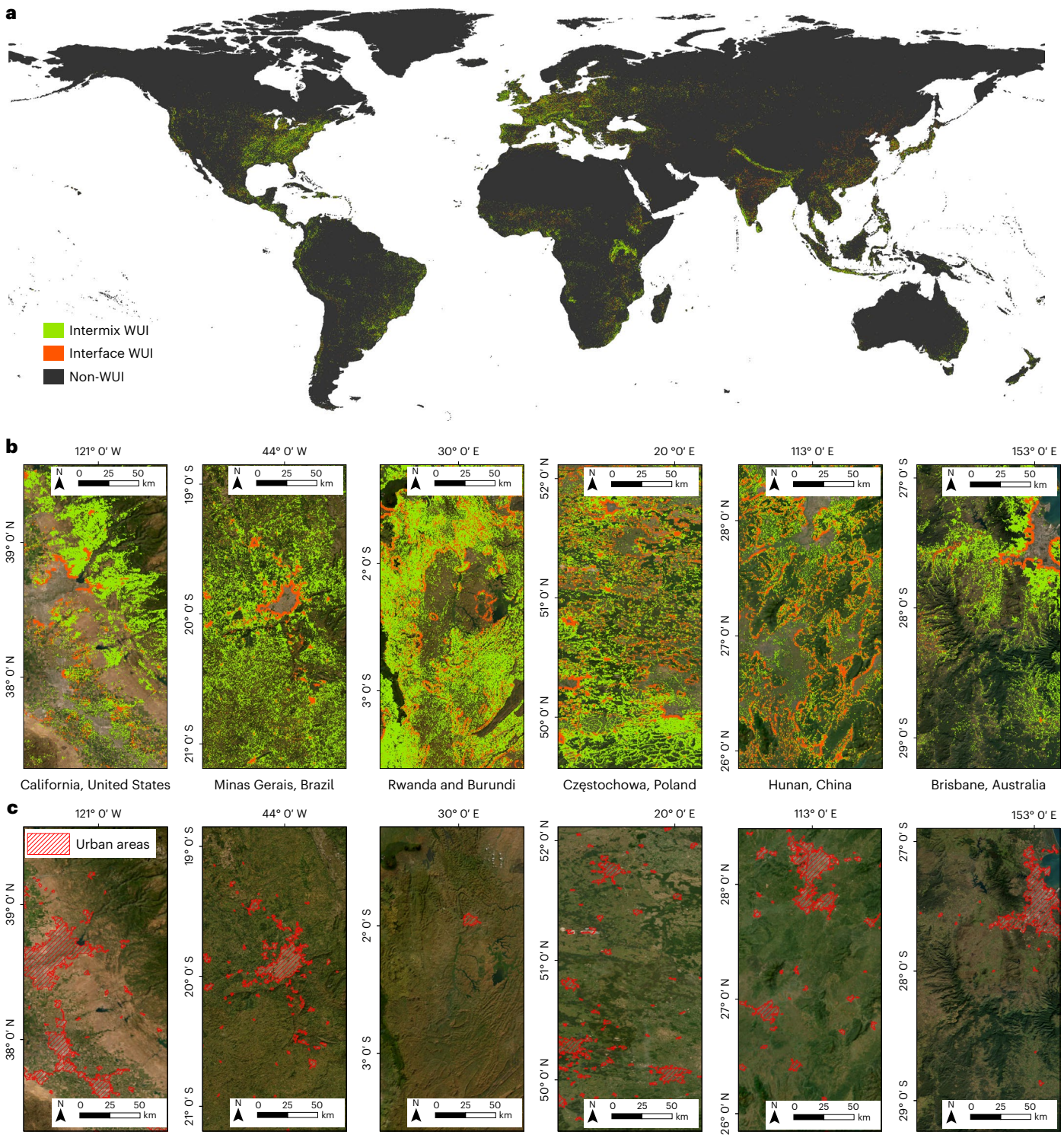

Fig. 1 | Global distribution of WUIs. a–**c**, Geographic distribution of global WUI areas (**a**) and zoomed-in subsets of intermix WUI and interface WUI areas (**b**) and global urban areas (**c**) overlaid on high-resolution satellite imagery across different continents in 2020. The administrative boundaries data are from the Global Administrative Areas database (GADM) (https://gadm.org/).

Historical evolution of global WUIs

Supplementary Fig. 8 presents the time-series global WUI maps at five-year intervals from 1985 to 2020 (with an R^2 of 0.78 compared to our mapped 2020 WUI baseline; Supplementary Fig. 9), differentiated by interface and intermix WUIs, with close-up examples of California and Australia's east coast in Fig. 3. We can observe significant variations in the spatiotemporal development of WUI areas across regions, even on local scales. Quantitative findings indicate a substantial increase of 12.56% in the global WUI area between 1985 and 2020. Of this total growth, interface WUIs made up the majority at 77.43%, with intermix WUIs accounting for the remaining 22.57%. Specifically, the interface WUIs expanded by 44.26% and the intermix WUIs by 3.63%, compared with their 1985 baselines. With an areal aggregation by continents (Fig. 4 and Supplementary Table 2), we found that Australia/Oceania

https://doi.org/10.1038/s41893-024-01291-0

Table 1 | WUIs at risk of wildfire across continents

Continent	Interface WUI (km^2)	Intermix WUI (km^2)	WUI (km^2)	Interface WUI within fires (%)	Intermix WUI within fires (%)	WUI within fires (%)	Interface WUI within 2.4 km buffer of fires (%)	Intermix WUI within 2.4 km buffer of fires (%)	WUI within 2.4 km buffer of fires (%)	Interface WUI within 4.8 km buffer of fires (%)	Intermix WUI within 4.8 km buffer of fires (%)	WUI within 4.8 km buffer of fires (%)
North America	266,505	1,146,407	1,412,912	0.04	0.11	0.10	1.48	1.87	1.80	4.00	4.72	4.58
South America	111,137	680,702	791,839	0.15	0.45	0.41	5.44	6.21	6.10	13.45	13.81	13.76
Europe	307,842	942,538	1,250,380	0.05	0.16	0.13	1.46	1.59	1.56	3.89	3.82	3.84
Africa	259,757	975,745	1,235,503	0.90	4.35	3.63	21.91	26.14	25.25	35.63	38.21	37.66
Asia	614,328	1,174,006	1,788,334	0.06	0.26	0.20	2.77	3.51	3.26	7.04	7.63	7.43
Australia/Oceania	17,941	120,337	138,278	0.11	0.40	0.36	3.16	3.25	3.23	7.67	6.95	7.04
Global	1,577,511	5,039,735	6,617,246	0.20	1.03	0.83	5.64	7.52	7.07	11.08	12.99	12.54

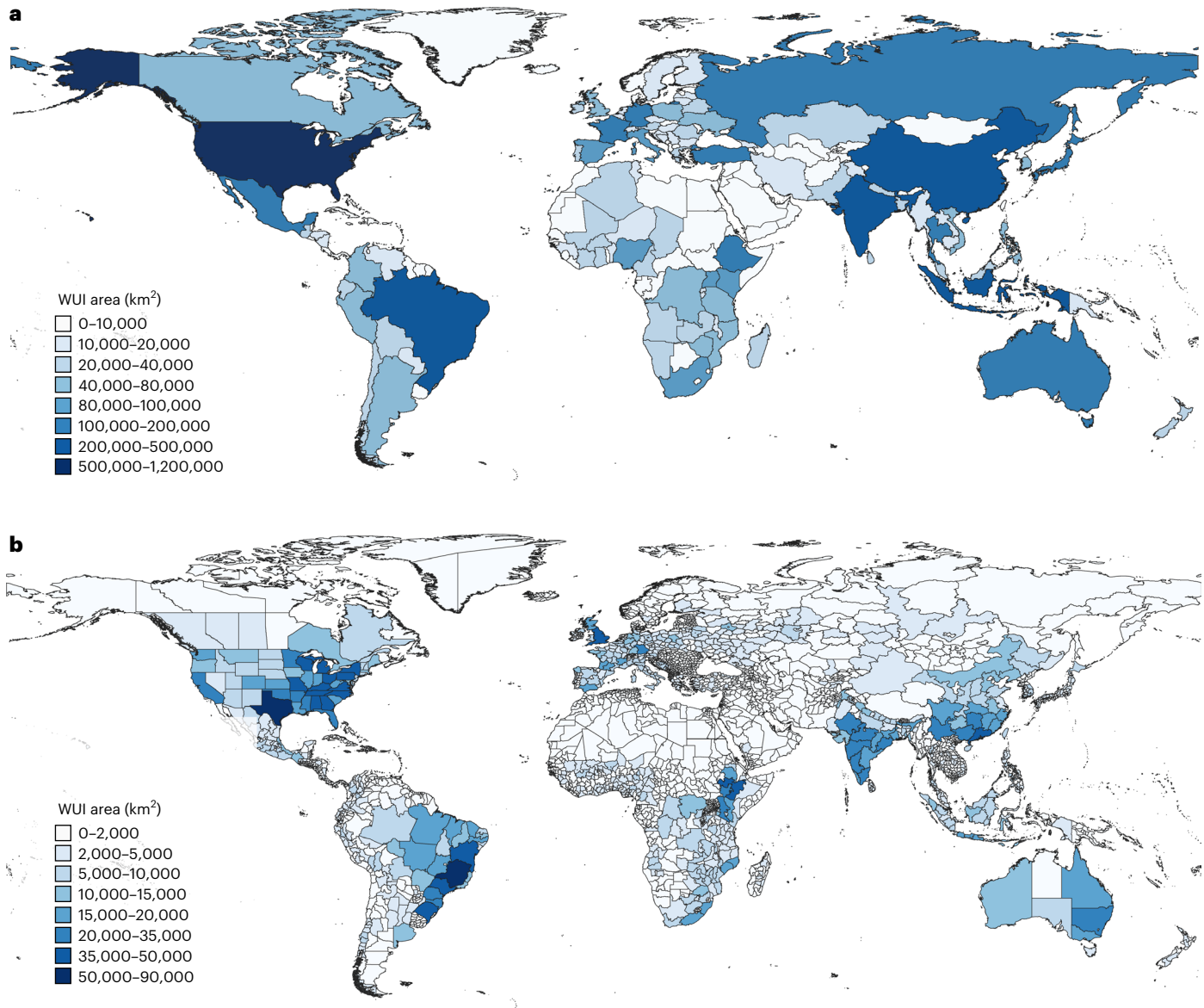

Fig. 2 | Global WUI area at the country and state levels. a,**b**, WUI areas including both interface and intermix WUI areas at the country level (**a**) and the state level (**b**) globally. The administrative boundaries data are from GADM (https://gadm.org/).

https://doi.org/10.1038/s41893-024-01291-0

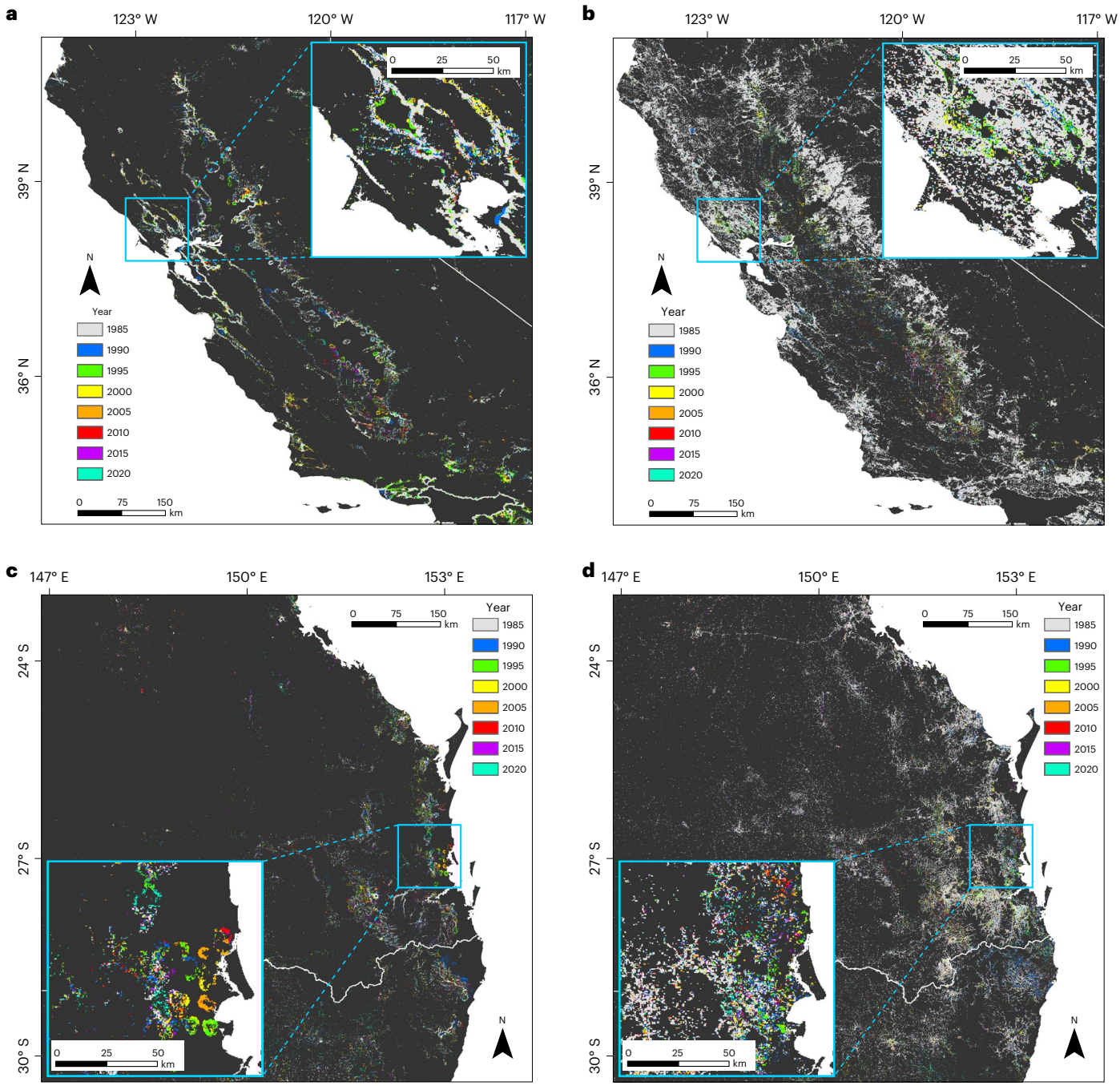

Fig. 3 | Spatiotemporal changes in global WUI areas. a–d, Spatiotemporal changes in global WUI areas at five-year intervals from 1985 to 2020, differentiated by interface WUIs (**a**,**c**) and intermix WUIs (**b**,**d**), using the examples of California (**a**,**b**) and Australia's east coast (**c**,**d**). The full change maps of global WUI areas are provided in Supplementary Fig. 8. The administrative boundaries data are from GADM (https://gadm.org/).

experienced the highest WUI area expansion at a rate of 27.81%, followed by Asia at 24.52%. Unlike other continents where interface WUI expansion dominates considerably, both Asia and Australia/Oceania witnessed notable intermix WUI expansions, specifically 12.14% for Asia and 18.91% for North America. It is worth noting that Africa experienced the highest growth rate of interface WUIs at 116.82%, followed by South America at 68.88%. When analysing by GFED regions (Supplementary Fig. 10 and Supplementary Table 3), Central America (31.60%), Southeast Asia (30.13%), and Australia and New Zealand (27.85%) witnessed considerable increases in total WUI area. In terms of specific WUI types, Southern Hemisphere Africa (143.10%), Northern Hemisphere Africa (106.63%) and Central America (93.80%) experienced the largest interface WUI expansions, while Equatorial Asia (28.38%), Southeast Asia (20.39%), and Australia and New Zealand (18.79%) saw the largest intermix WUI expansions.

Wildfire risk in WUI areas

By overlaying the fine-resolution footprints of 2020 WUI (Fig. 1), wildfires and population, we estimated spatially explicit WUI areas globally that are under threat of wildfire (Fig. 5). We also estimated the wildfire-exposed population within WUI areas (Supplementary Table 4). Between 2001 and 2020, we observed that an average of 0.83% of WUI areas worldwide experienced wildfires, directly exposing 0.27 million people to this threat (Table 1 and Supplementary Table 4).

https://doi.org/10.1038/s41893-024-01291-0

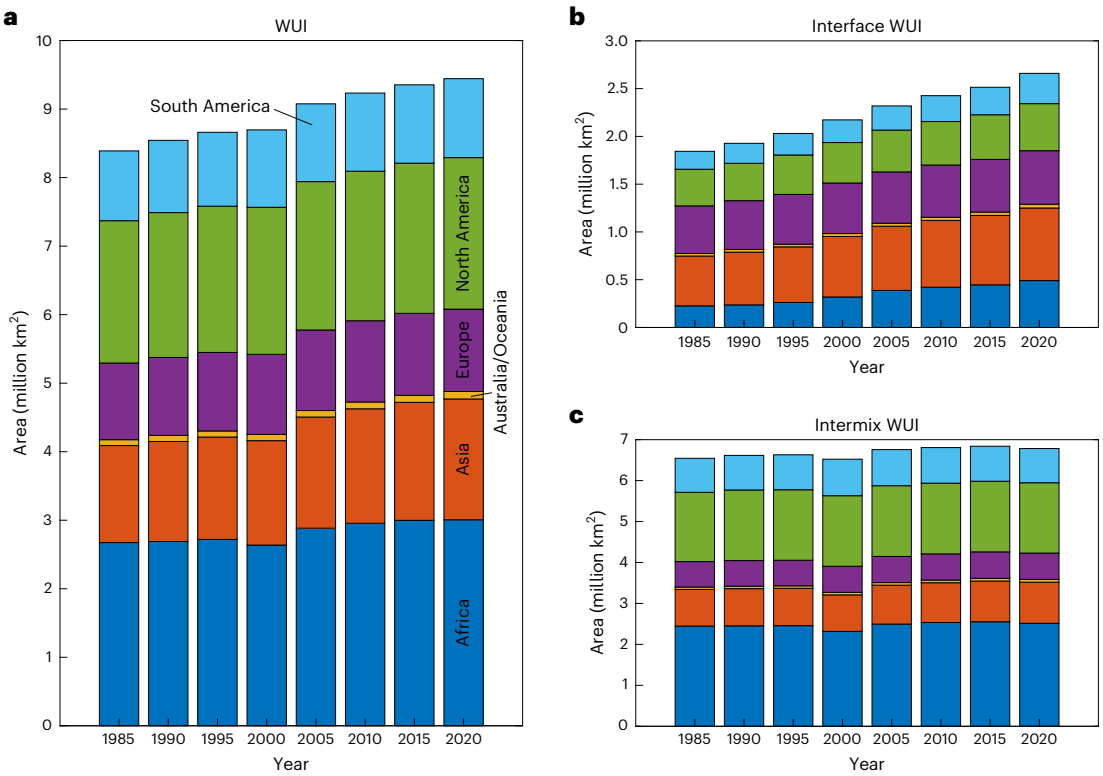

Fig. 4 | Temporal changes in global WUI areas. a–**c**, Temporal changes in total WUIs (**a**), interface WUIs (**b**) and intermix WUIs (**c**) across continents from 1985 to 2020.

A detailed examination reveals that 7.07% and 12.54% of WUI areas are within 2,400 m and 4,800 m buffer zones of wildfire threat; these areas house approximately 4.47 million and 10.11 million people, respectively (Table 1 and Supplementary Table 4).

In comparison with interface WUI areas, intermix WUI areas are exposed to higher wildfire risk (Table 1). Globally, 1.03% of intermix WUI areas experienced wildfires during the study period, which is a much higher proportion than for interface WUI areas (0.20%). Within the 2,400 m and 4,800 m buffer zones, intermix WUI areas (7.52% and 12.99%, respectively) consistently experienced higher wildfire risk than interface WUI areas (5.64% and 11.08%, respectively).

We found that Africa has the highest WUI wildfire risk, followed by South America, Asia, Australia/Oceania, North America and Europe (Table 1). This contrasting pattern was also statistically verified at both the country and state levels (Fig. 5 and Supplementary Fig. 11). In Africa, 3.63% of WUI areas burned during 2001–2020, with 0.21 million people (1.08% of the total population within the WUI areas) directly exposed to the threat of wildfire; moreover, 25.25% and 37.66% of WUI areas were in the 2,400 m and 4,800 m buffer zones, exposing 2.74 million and 5.07 million people (13.92% and 25.72% of the total population, respectively) to the threat of wildfire (Supplementary Table 4). In North America, only 0.27% of WUI areas experienced wildfires during the study period (5.42% and 12.79% of the WUI areas were in the surrounding 2,400 m and 4,800 m buffer zones, respectively) (Table 1). However, some US states, such as Kansas (4.91%), Louisiana (3.23%), California (2.16%) and Nevada (2.08%), are at higher risk of wildfires within the 2,400 m buffer zone of their WUI areas (Fig. 5b). Data on the population living within WUIs exposed to risk of wildfire across GFED regions are provided in Supplementary Table 5.

Discussion

The rapid encroachment of human settlements into wildland areas has exacerbated wildfire challenges in WUI areas[18,19,21]. Previous studies have highlighted the widespread extent of the WUI in countries including the United States, Argentina, Australia, France and South Africa. Knowledge of the distribution and composition of WUIs is essential for shaping fire management strategies, fostering fire-resilient communities and informing insurance regulations[23,31]. In this study, we extended WUI mapping to the global context by characterizing the fine-resolution footprints of houses and vegetation to produce reliable and spatially explicit WUI mapping for the 2020 baseline and the 1985–2020 time series. This dataset offers new and comprehensive information on both interface and intermix WUI areas, facilitating more detailed analyses to advance the field of WUI-related wildfire management and provide valuable insight into future research, policymaking, planning and management. We highlight three major points regarding the advantage of WUI mapping. First, we applied the general definition of the WUI to generate globally consistent mapping results, allowing reliable comparisons and assessments across regions and countries. This approach, which represents a robust complement to existing WUI mapping studies at local and country levels, helps advance understanding of the global WUI distribution. Second, unlike WUI products derived using a zonally based approach[18,21], we adopted the point-based approach with fine-resolution satellite-based housing footprint and vegetation data to derive the spatial extent of WUI areas, which enables the delineation of more detail in the spatial coverage and configuration of WUI areas[32] (Supplementary Fig. 2). Such refined WUI information will be critically important for supporting local management actions such as fuel treatment and evacuation response, as well as aggregating up for better-discriminated national, regional and global policies and practices. Third, the temporally consistent and fine-resolution mappings of land-cover types and human settlement used in this study enable the long-term tracing of global WUI dynamics over the past 35 years. The availability of historical time series of WUI products could help improve understanding of the biophysical and socio-economic drivers of change in the WUI spatially and over time, enhance the detection of the response of wildfire risk to the changing WUI, and

https://doi.org/10.1038/s41893-024-01291-0

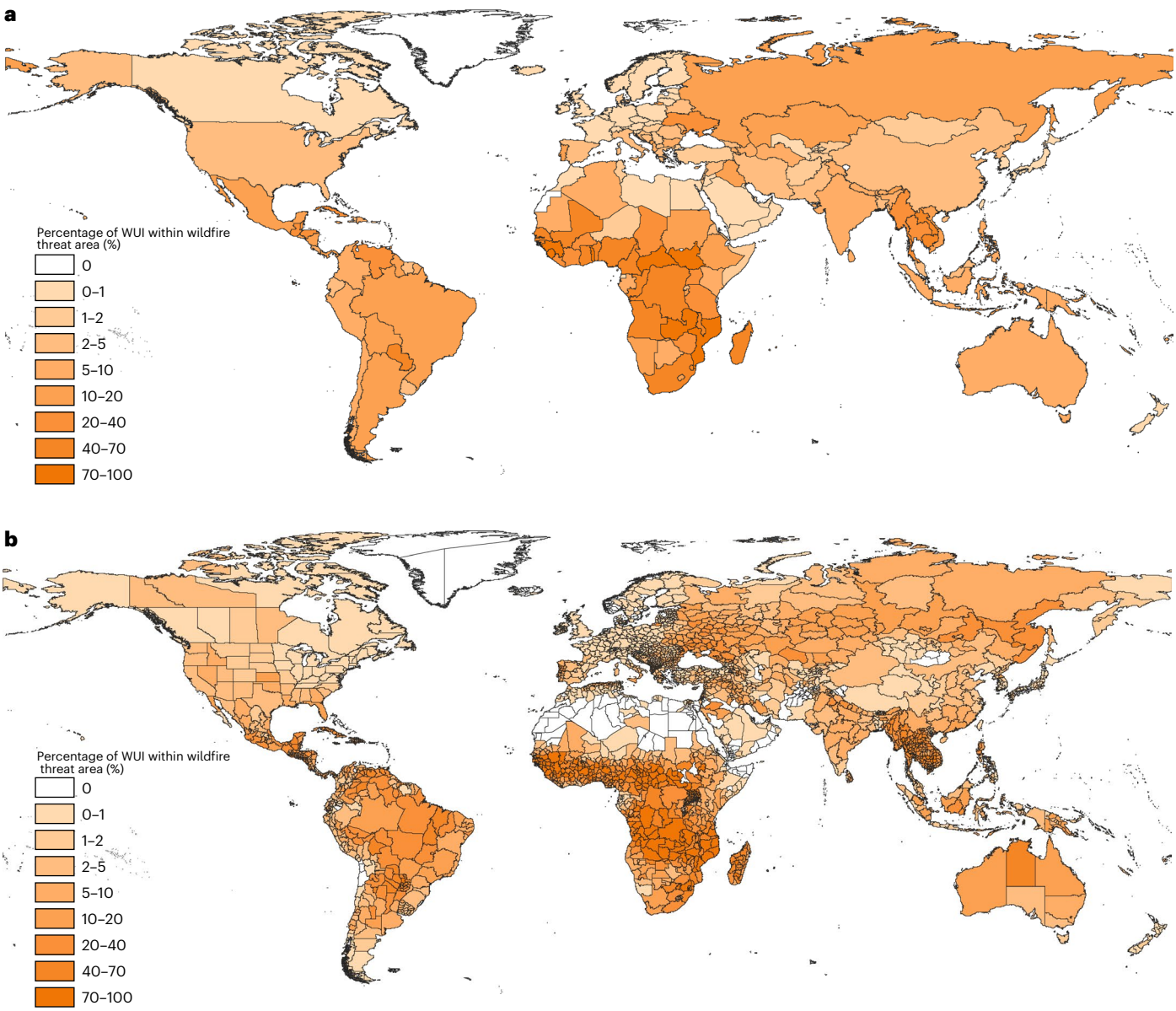

Fig. 5 | WUI areas within wildfire threat areas. a,**b**, The percentage of WUI areas within the 2,400 m buffer areas of wildfire threat during 2001–2020 on average at the country level (**a**) and state level (**b**) globally. The administrative boundaries data are from GADM (https://gadm.org/).

support sustainable pathways of settlement development, wildlife conservation and wildfire management.

Our analysis quantitatively evaluated the wildfire risk for global WUI areas. Global estimates reveal that 0.83% of WUI areas on average experienced wildfires during 2001–2020. This means that at least 0.34 million houses (estimated using the minimum threshold of housing density of >1 house per 0.16 km^2) were exposed to wildfire risk. More alarming is the fact that 7.07% and 12.54% of WUI areas (at least 2.92 million and 5.19 million houses) are within 2,400 m and 4,800 m buffer zones of wildfire threat, respectively. Although these WUI regions have certain protective buffer distances from wildfire burned areas, they remain highly vulnerable to air pollution and wildfire spread under extreme weather conditions. The ever-expanding WUI is expected to result in increased wildfire ignition[18], which means that current and future WUI areas will be exposed to enhanced risk of wildfire. Globally, we identified a contrasting pattern in the spatial distribution of WUI areas and associated wildfire risk. The majority of WUI areas are distributed in the United States, Brazil, China, India and Australia (Fig. 2). However, African countries have much higher rates of wildfire risk in their WUI areas (Fig. 5a) because of the intensified wildfire regimes[9]. Human activity can both intensify (via increasing density of ignitions) and weaken (via forcing wildfire suppression or prevention) wildfires in WUI areas. This duality affects the geographical distribution of wildfire risk in WUI areas. The areas with largest risk in Africa and South America are where the density of ignition is highest and fire duration is longest[33]; in the Asian part of Russia and northern Australia, the largest risk is due to insufficient fire suppression. Both ignition density and fire duration are low (owing to the prevention and suppression of wildfires) in highly urbanized Europe and North America[33], resulting in low risk of wildfire in their WUI areas. The derived spatially explicit dataset outlining the geographic distribution of WUI areas and the associated wildfire risk, particularly vulnerable WUIs under serious threat of wildfires, is expected to have broad practical implications for potential beneficiaries.

Our study improves the understanding of the spatiotemporal patterns of WUI areas and the associated wildfire risk globally, but we recognize that some uncertainties remain. First, we combined the High Resolution Population Density (HRPD) and World Settlement Footprint

(WSF) datasets to characterize house footprints globally because of data availability. Certain intrinsic mismatches exist between these two datasets—for example, the WSF product tends to underestimate isolated housing structures. With further updating of the Meta (formerly Facebook) HRPD dataset, our WUI products will be updated for those countries when the HRPD dataset becomes available. Another source of data uncertainty is the MODIS wildfire occurrence. Although we used the Terra and Aqua combined MCD64A1 Burned Area datasets from 2001–2020 to represent the average status of wildfire regimes, short-term or smaller fires occurring in WUI areas may be missed due to the coarse-resolution satellite-based observations. This could lead to underestimates of wildfire risks in certain regions. Combining multi-source remote sensing datasets, including MODIS, VIIRS and Geostationary satellites such as NOAA's Geostationary Operational Environmental Satellite, would be promising to better consolidate the wildfire inventory within a spatially and temporally explicit context. Second, we used the same definition of WUI as published by the US government in the Federal Register[34]. Although this definition has been adopted widely in the field of WUI assessment, some studies have highlighted that the WUI will differ between locations, especially in relation to the optimal thresholds of the distance parameter, housing density and vegetation amount[32,35]. Another major uncertainty embedded in WUI mapping is the vegetation definition. For example, including or excluding shrubs and grasses in the vegetation for WUI mapping can lead to a considerable difference in the final distribution of WUI areas (Supplementary Figs. 12 and 13, Supplementary Tables 6 and 7, and Supplementary Information). Users of our global WUI maps are therefore recommended to conduct a preliminary check to ensure that the maps are robust to different local spatial contexts. In particular, we emphasize the need to calibrate local maps for topological, service-provision and other determinants of fire suppression, and with local meteorological data. Third, while this study is among the pioneering attempts to create time-series dynamics of global WUI mapping, the spatial details of natural vegetation and human settlement used to delineate WUI distributions have coarser resolutions of 30 m and 100 m, respectively, than our baseline WUI mapping for 2020. The decreased spatial resolution of the sourced datasets might result in certain biases when mapping microscale WUI areas, considering the heterogeneous landscape of both interface and intermix WUI types. Meanwhile, the time-series vegetation and human settlement layers we used have reported relatively plausible accuracies[36,37]. However, unavoidable biases embedded in their temporal consistency may also result in potential uncertainties when reconstructing the historical evolution of WUI areas.

Regardless of the inherent uncertainty in this study, our analysis offers a comprehensive understanding of the spatiotemporal patterns of WUI areas globally, with a particular focus on the wildfire risks estimated across regions. By shedding light on the composition and heterogeneities of global WUI areas and the associated wildfire risk, the study can enable policymakers and stakeholders to better allocate resources and implement targeted measures for protecting vulnerable communities. Furthermore, the evidence gained here can inform land-use planning and development decisions, promoting sustainable urban growth while mitigating wildfire risk.

Methods

Housing footprint

The WUI represents the area where houses and wildland vegetation either intermingle or abut. Quantification of houses and vegetation therefore represents the two essential components for generating reliable WUI maps. We used the 30 m building footprint from the Meta (formerly Facebook) HRPD maps to quantify the spatial distribution and density of housing[38]. The HRPD maps represent the most accurate population datasets on a 30 m × 30 m grid (that is, building footprint), which are derived from integration of high-resolution (0.5 m) commercial satellite images (DigitalGlobe), large-scale OpenStreetMap label data, state-of-the-art computer vision techniques and Center for International Earth Science Information Network Gridded Population of the World data[38].

For countries without available HRPD maps, including Afghanistan, Canada, China, Cuba, Greenland, Morocco, Myanmar, North Korea, Russia, Somalia, Sudan, Syria, Ukraine, Venezuela and Yemen, we used the 10 m WSF map[39] to delineate human settlement locations. The WSF map is generated by integrating open-and-free optical and radar satellite (Sentinel-1 and Landsat-8) imagery and the robust classifier of the support vector machine with the radial basic function Gaussian kernel. Validation using 900,000 samples from crowdsourcing photointerpretation of very-high-resolution Google Earth imagery revealed that the WSF map has remarkably higher accuracy than other similar human settlement products[39] such as the Global Urban Footprint[40], Global Human Settlement Layer[41] and GlobeLand30 products[42]. In particular, the WSF map considerably improves the detection of very small settlements in rural regions and scattered suburban areas[39].

Wildland vegetation

We used the European Space Agency's latest global baseline land-cover product for 2020 (WorldCover) with 10 m spatial resolution to quantify the spatial distribution of wildland vegetation. The WorldCover map includes 11 different land-cover classes with an overall accuracy of 75% globally[43]. The combined use of Sentinel-1 and Sentinel-2 satellite data not only enhances the spatial resolution of the WorldCover map to 10 m but also provides reliable land-cover information in areas with persistent cloud cover[43]. We first extracted all types of forest, shrub and grass from the WorldCover maps as wildland vegetation. To exclude vegetation that is clearly not wild, such as urban green space and human-induced plantations, we used the global urban boundary[44], extracted from the 30 m Landsat-derived impervious area in 2018, and the 10 m global industrial and smallholder oil palm map for 2019[45] to remove all urban green space and oil palm plantations from the baseline wildland vegetation layer.

Mapping and validating the WUI

We adopted the WUI definition as published by the US government in the Federal Register[34], which has been used widely in the field of WUI mapping and assessment[18,20,35]. The definition specifies two types of WUI: intermix and interface. The intermix WUI is where houses and wildland vegetation intermingle, with a housing density of >1 house per 40 acres (~160,000 m^2) and where >50% of the area is covered by wildland vegetation. The interface WUI represents housing areas (>1 house per 40 acres) with <50% coverage of wildland vegetation but lying within 2.4 km of a densely vegetated area (>75% wildland vegetation) that is at least 5 km^2 in size[18].

Given the housing density threshold of >1 house per 160,000 m^2 (that is, 1 house per 400 m × 400 m grid), the spatial resolution of 400 m was chosen as the minimum unit of our WUI mapping. We aggregated the 30 m building footprint maps and 10 m WSF map to 400 m grids to calculate housing density. Similarly, we aggregated the 10 m wildland vegetation maps to 400 m grids to calculate the percentage vegetation coverage. We first identified all intermix WUI areas by overlapping the 400 m housing density maps and percentage wildland vegetation coverage maps on the basis of the housing (>1) and vegetation (>50%) thresholds. We then identified interface WUI areas through the following steps: (1) selecting contiguous vegetation patches >5 km^2 in size and with >75% wildland vegetation coverage, (2) generating a 2.4 km outside buffer area based on the vegetation areas selected in step 1, (3) identifying housing areas with >1 house per 40 acres and with <50% wildland vegetation coverage, and (4) extracting the overlapped areas determined in steps 2 and 3 as the interface WUI.

We collected the WUI map for 2010 in the conterminous United States derived from census block data and the US Geological Survey National Land Cover Database[18], and compared it with our newly generated WUI data in terms of the interface WUI, intermix WUI and total WUI at the state level. We also collected the recently released global 10 m WUI map for 2020[29] and compared it with our new one in terms of the interface WUI, intermix WUI and total WUI at the state level. We used linear regression to check the correlation between these comparable products, and we used the derived R^2 value as a quantitative measure for validating mapping performance.

Mapping time-series dynamics of global WUI areas

By using the same WUI definition, we integrated two temporally consistent datasets of land cover and human settlements to produce time-series global WUI maps at five-year intervals from 1985 to 2020. Specifically, we employed the 30 m global land-cover product with fine classification system (GLC-FCS)[36] and 100 m global human settlement layers[37]. For the GLC-FCS product, we identified forest, shrubland and grassland as natural vegetation. Similarly, to exclude vegetation that is clearly not wild, such as urban green space and human-induced plantations, we used the time-series global urban boundaries[44], extracted from the 30 m Landsat-derived impervious area from 1990 to 2018, and the 10 m global industrial and smallholder oil palm map for 2019[45] to remove all urban green space and oil palm plantations from the baseline wildland vegetation layer. We applied the same methodology for extracting interface and intermix WUIs as detailed above for the 2020 baseline mapping to generate time-series global WUI maps. For validation purposes, we incorporated our 2020 baseline WUI map as a benchmark and compared it to the 2020 WUI map from the time-series product in terms of interface WUI, intermix WUI and total WUI at the state level. We employed linear regression to examine the correlation between these two products, and we used the derived R^2 value as a quantitative measure to validate mapping performance.

Wildfire risk for WUI areas

We collected the Terra and Aqua combined MCD64A1 Version 6 Burned Area data product to quantify the geographic distribution of global wildfire regimes during 2001–2020. The MCD64A1 is a monthly, global gridded 500 m product containing per-pixel burned area and has been used widely to characterize global wildfire dynamics[46]. We first summed the monthly burned area for a given calendar year using the date of burn for the 500 m grid cells to represent the spatial niche of fires for each year. We then generated two outside buffer zones for each burned area using a radius of 2,400 and 4,800 m to represent potential wildfire risk areas. The distance of 2,400 m (~1.5 miles) represents an average estimate of how far a firebrand can spread from a fire front, which is a rationale related to fire policy application[47]. We therefore used one and two times this empirical distance to represent two scenarios for wildfire risk assessment. Finally, we overlapped the original wildfire burned areas and potential wildfire risk areas in the 2,400 m and 4,800 m buffers with our derived WUI maps to estimate the WUI areas under threat of wildfire. On the basis of the spatially explicit map of WUI–wildfire interaction, we further calculated the proportion of the WUI as an entire unit and differentiated it in terms of the interface WUI and intermix WUI at risk of wildfire globally and across countries.

Population exposed to wildfires in WUI areas

We incorporated the spatially and temporally explicit WorldPop population dataset to estimate the population exposed to the risk of wildfire in WUI areas. WorldPop provides an estimate of the number of people residing in each 100 m × 100 m grid based on a random forest model and a global database of administrative-unit-based census information[48], which has much finer spatial resolution and higher update frequency than other population datasets such as the Gridded Population of the World[49] and LandScan datasets[50]. Specifically, we intersected the population and WUI areas to achieve the spatially explicit population distribution in the WUIs, and then overlapped it with wildfire burned areas during 2001–2020 to calculate a suite of estimates that included the population within the WUIs and the wildfire-exposed population within the WUIs using three scenarios: direct impact, 2,400 m buffer impact and 4,800 m buffer impact. Statistics were estimated in terms of the entire WUI, interface WUI and intermix WUI at the GFED region level and at both country and state levels.

Reporting summary

Further information on research design is available in the Nature Portfolio Reporting Summary linked to this article.

Data availability

The global hierarchy of administrative unit layers are from the Food and Agriculture Organization of the United Nations (https://data.apps.fao.org). The population dataset is from WorldPop (https://www.worldpop.org). The global baseline land-cover product for 2020 (WorldCover) is from the European Space Agency (https://esa-worldcover.org). The Meta (formerly Facebook) HRPD maps are from the Data for Good platform (https://dataforgood.facebook.com/dfg/tools/high-resolution-population-density-maps). The WSF maps are from the Scientific Data repository (https://www.nature.com/articles/s41597-020-00580-5). The wildfire burned area datasets are from the MODIS data archive in Google Earth Engine (https://earthengine.google.com). The global urban area boundaries are from the FROM-GLC research group (https://data-starcloud.pcl.ac.cn/). The global industrial and smallholder oil palm map is from Zenodo (https://zenodo.org/record/4473715). WUI data in the United States for validation are from the SILVIS lab (http://silvis.forest.wisc.edu/data/wui-change). The 30 m GLC-FCS product is from Zenodo (https://zenodo.org/record/3986872). The 100 m global human settlement layers are from the Joint Research Centre of the European Commission (https://ghsl.jrc.ec.europa.eu/ghs_buS2023.php). The global WUI datasets for the 2020 baseline and 1985–2020 time series have been deposited in the following repository: https://datahub.hku.hk/projects/GlobalWUI/191163.

References

1. Bond, W. J., Woodward, F. I. & Midgley, G. F. The global distribution of ecosystems in a world without fire. *N. Phytol.* **165**, 525–538 (2005).
2. Wu, C. et al. Reduced global fire activity due to human demography slows global warming by enhanced land carbon uptake. *Proc. Natl Acad. Sci. USA* **119**, e2101186119 (2022).
3. Jin, Y. et al. Identification of two distinct fire regimes in Southern California: implications for economic impact and future change. *Environ. Res. Lett.* **10**, 094005 (2015).
4. Johnston, F. H. et al. Estimated global mortality attributable to smoke from landscape fires. *Environ. Health Perspect.* **120**, 695–701 (2012).
5. Sanderfoot, O. V. et al. A review of the effects of wildfire smoke on the health and behavior of wildlife. *Environ. Res. Lett.* **16**, 123003 (2021).
6. *Spreading like Wildfire: The Rising Threat of Extraordinary Landscape Fires—a UNEP Rapid Response Assessment, Nairobi* (United Nations Environment Programme, 2022).
7. Yu, Y. et al. Machine learning–based observation-constrained projections reveal elevated global socioeconomic risks from wildfire. *Nat. Commun.* **13**, 1250 (2022).
8. Chen, B. et al. Climate, fuel, and land use shaped the spatial pattern of wildfire in California's Sierra Nevada. *J. Geophys. Res. Biogeosci.* **126**, e2020JG005786 (2021).
9. Andela, N. et al. A human-driven decline in global burned area. *Science* **356**, 1356–1362 (2017).

10. Gutierrez Aurora, A. et al. Wildfire response to changing daily temperature extremes in California's Sierra Nevada. *Sci. Adv.* **7**, eabe6417 (2021).
11. Westerling, A. L., Hidalgo, H. G., Cayan, D. R. & Swetnam, T. W. Warming and earlier spring increase western U.S. forest wildfire activity. *Science* **313**, 940–943 (2006).
12. Williams, A. P. et al. Observed impacts of anthropogenic climate change on wildfire in California. *Earth's Future* **7**, 892–910 (2019).
13. Mueller, S. E. et al. Climate relationships with increasing wildfire in the southwestern US from 1984 to 2015. *Ecol. Manage.* **460**, 117861 (2020).
14. Holden, Z. A. et al. Decreasing fire season precipitation increased recent western US forest wildfire activity. *Proc. Natl Acad. Sci. USA* **115**, E8349–E8357 (2018).
15. Stephens, S. L. et al. Drought, tree mortality, and wildfire in forests adapted to frequent fire. *Bioscience* **68**, 77–88 (2018).
16. Gudmundsson, L., Rego, F. C., Rocha, M. & Seneviratne, S. I. Predicting above normal wildfire activity in southern Europe as a function of meteorological drought. *Environ. Res. Lett.* **9**, 084008 (2014).
17. Chen, B. & Jin, Y. Spatial patterns and drivers for wildfire ignitions in California. *Environ. Res. Lett.* **17**, 055004 (2022).
18. Radeloff, V. C. et al. Rapid growth of the US wildland–urban interface raises wildfire risk. *Proc. Natl Acad. Sci. USA* **115**, 3314–3319 (2018).
19. Balch, J. K. et al. Human-started wildfires expand the fire niche across the United States. *Proc. Natl Acad. Sci. USA* **114**, 2946–2951 (2017).
20. Radeloff, V. C. et al. The wildland–urban interface in the United States. *Ecol. Appl.* **15**, 799–805 (2005).
21. Theobald, D. M. & Romme, W. H. Expansion of the US wildland–urban interface. *Landsc. Urban Plan.* **83**, 340–354 (2007).
22. Zhang, Y., He, H. S. & Yang, J. The wildland–urban interface dynamics in the southeastern US from 1990 to 2000. *Landsc. Urban Plan.* **85**, 155–162 (2008).
23. Calkin, D. E., Cohen, J. D., Finney, M. A. & Thompson, M. P. How risk management can prevent future wildfire disasters in the wildland–urban interface. *Landsc. Urban Plan.* **111**, 746–751 (2014).
24. Johnston, L. M. & Flannigan, M. D. Mapping Canadian wildland fire interface areas. *Int. J. Wildland Fire* **27**, 1–14 (2017).
25. Koksal, K., McLennan, J., Every, D. & Bearman, C. Australian wildland–urban interface householders' wildfire safety preparations: 'Everyday life' project priorities and perceptions of wildfire risk. *Int. J. Disaster Risk Reduct.* **33**, 142–154 (2019).
26. Alcasena, F. J., Evers, C. R. & Vega-Garcia, C. The wildland–urban interface raster dataset of Catalonia. *Data Br.* **17**, 124–128 (2018).
27. Lampin-Maillet, C. et al. Mapping wildland–urban interfaces at large scales integrating housing density and vegetation aggregation for fire prevention in the South of France. *J. Environ. Manage.* **91**, 732–741 (2010).
28. Bento-Gonçalves, A. & Vieira, A. Wildfires in the wildland–urban interface: key concepts and evaluation methodologies. *Sci. Total Environ.* **707**, 135592 (2020).
29. Schug, F. et al. The global wildland–urban interface. *Nature* **621**, 94–99 (2023).
30. *Climate Risk Map of Australia* (Climate Council, 2022).
31. Schoennagel, T. et al. Adapt to more wildfire in western North American forests as climate changes. *Proc. Natl Acad. Sci. USA* **114**, 4582–4590 (2017).
32. Bar-Massada, A. A comparative analysis of two major approaches for mapping the wildland–urban interface: a case study in California. *Land* **10**, 679 (2021).
33. Andela, N. et al. The Global Fire Atlas of individual fire size, duration, speed and direction. *Earth Syst. Sci. Data* **11**, 529–552 (2019).
34. Glickman, D. & Babbitt, B. Urban wildland interface communities within the vicinity of federal lands that are at high risk from wildfire. *Fed. Regist.* **66**, 751–777 (2001).
35. Bar-Massada, A., Stewart, S. I., Hammer, R. B., Mockrin, M. H. & Radeloff, V. C. Using structure locations as a basis for mapping the wildland urban interface. *J. Environ. Manage.* **128**, 540–547 (2013).
36. Zhang, X. et al. GLC_FCS30: global land-cover product with fine classification system at 30 m using time-series Landsat imagery. *Earth Syst. Sci. Data* **13**, 2753–2776 (2021).
37. Pesaresi, M. & Politis, P. *GHS-BUILT-S R2023A—GHS Built-Up Surface Grid, Derived from Sentinel2 Composite and Landsat, Multitemporal (1975–2030)* (European Commission, Joint Research Centre, 2023).
38. *High Resolution Population Density Maps* (Facebook and Columbia University—CIESIN, 2022).
39. Marconcini, M. et al. Outlining where humans live, the World Settlement Footprint 2015. *Sci. Data* **7**, 242 (2020).
40. Esch, T. et al. Breaking new ground in mapping human settlements from space—the Global Urban Footprint. *ISPRS J. Photogramm. Remote Sens.* **134**, 30–42 (2017).
41. Corbane, C. et al. Automated global delineation of human settlements from 40 years of Landsat satellite data archives. *Big Earth Data* **3**, 140–169 (2019).
42. Chen, J. et al. Global land cover mapping at 30 m resolution: a POK-based operational approach. *ISPRS J. Photogramm. Remote Sens.* **103**, 7–27 (2015).
43. Zanaga, D. et al. *ESA WorldCover 10 m 2020* v.100 (European Space Agency WorldCover consortium, 2021).
44. Li, X. et al. Mapping global urban boundaries from the global artificial impervious area (GAIA) data. *Environ. Res. Lett.* **15**, 094044 (2020).
45. Descals, A. et al. High-resolution global map of smallholder and industrial closed-canopy oil palm plantations. *Earth Syst. Sci. Data* **13**, 1211–1231 (2021).
46. Giglio, L., Boschetti, L., Roy, D. P., Humber, M. L. & Justice, C. O. The Collection 6 MODIS burned area mapping algorithm and product. *Remote Sens. Environ.* **217**, 72–85 (2018).
47. Stewart, S. I., Radeloff, V. C., Hammer, R. B. & Hawbaker, T. J. Defining the wildland–urban interface. *J. For.* **105**, 201–207 (2007).
48. Stevens, F. R., Gaughan, A. E., Linard, C. & Tatem, A. J. Disaggregating census data for population mapping using random forests with remotely-sensed and ancillary data. *PLoS ONE* **10**, e0107042 (2015).
49. CIESIN *Gridded Population of the World, Version 4 (GPWv4): Population Count, Revision 11* (NASA Socioeconomic Data and Applications Center, 2018).
50. Dobson, J. E., Bright, E. A., Coleman, P. R., Durfee, R. C. & Worley, B. A. LandScan: a global population database for estimating populations at risk. *Photogramm. Eng. Remote Sens.* **66**, 849–857 (2000).

Acknowledgements

This work was supported by the National Key Research and Development Program of China (grant no. 2022YFB3903703 to B.C. and B.X.), the University of Hong Kong HKU-100 Scholars Fund (to B.C.), the Research Grants Council of Hong Kong Early Career Scheme (grant no. HKU27600222 to B.C.) and General Research Fund (grant no. HKU17601423 to B.C.), University Research Committee Seed Funding for Strategic Interdisciplinary Research Scheme (to B.C.), the National Natural Science Foundation of China/RGC Joint Research Scheme (grant no. N_HKU722/23 to B.C. and S.W.), the Faculty of Business and Economics and Shenzhen Research Institutes (grant no. SZRI2023-CRF-04 to B.C.), the Croucher Foundation (grant no. CAS22902/CAS22HU01 to P.G.), the International Research Center of Big Data for Sustainable

Development Goals (grant nos CBAS2022GSP04 to P.G. and CBAS2022ORP02 to B.X.) and the Major Program of the National Natural Science Foundation of China (grant no. 42090015 to P.G.). S.V. acknowledges support from the Russian State Assignment of the Federal Research Centre, Southern Scientific Centre of the Russian Academy of Sciences (grant no. 122013100131-9).

Author contributions

B.C. conceived the research idea, designed the study, performed the main data analysis and wrote the manuscript. S.W. contributed to data collection. S.W., Y.J., Y.S., C. Wu, S.V., B.X., C. Webster and P.G. contributed to result interpretation and reviewed and edited the manuscript.

Competing interests

The authors declare no competing interests.

Additional information

Supplementary information The online version contains supplementary material available at https://doi.org/10.1038/s41893-024-01291-0.

Correspondence and requests for materials should be addressed to Bin Chen.

Peer review information *Nature Sustainability* thanks Antonio Bento-Gonçalves, Hong S. He and Jiafu Mao for their contribution to the peer review of this work.

nature portfolio

Corresponding author(s): Bin Chen

Last updated by author(s): Dec 31, 2023

Reporting Summary

Nature Portfolio wishes to improve the reproducibility of the work that we publish. This form provides structure for consistency and transparency in reporting. For further information on Nature Portfolio policies, see our Editorial Policies and the Editorial Policy Checklist.

Statistics

For all statistical analyses, confirm that the following items are present in the figure legend, table legend, main text, or Methods section.

n/a	Confirmed
☐	☒ The exact sample size (*n*) for each experimental group/condition, given as a discrete number and unit of measurement
☐	☒ A statement on whether measurements were taken from distinct samples or whether the same sample was measured repeatedly
☒	☐ The statistical test(s) used AND whether they are one- or two-sided *Only common tests should be described solely by name; describe more complex techniques in the Methods section.*
☐	☒ A description of all covariates tested
☒	☐ A description of any assumptions or corrections, such as tests of normality and adjustment for multiple comparisons
☐	☒ A full description of the statistical parameters including central tendency (e.g. means) or other basic estimates (e.g. regression coefficient) AND variation (e.g. standard deviation) or associated estimates of uncertainty (e.g. confidence intervals)
☒	☐ For null hypothesis testing, the test statistic (e.g. *F*, *t*, *r*) with confidence intervals, effect sizes, degrees of freedom and *P* value noted *Give P values as exact values whenever suitable.*
☒	☐ For Bayesian analysis, information on the choice of priors and Markov chain Monte Carlo settings
☒	☐ For hierarchical and complex designs, identification of the appropriate level for tests and full reporting of outcomes
☒	☐ Estimates of effect sizes (e.g. Cohen's *d*, Pearson's *r*), indicating how they were calculated

Our web collection on statistics for biologists contains articles on many of the points above.

Software and code

Policy information about availability of computer code

Data collection	No software was used in the data collection.
Data analysis	We used Google Earth Engine Platform 2023 and Matlab 2020b to analyze data.

For manuscripts utilizing custom algorithms or software that are central to the research but not yet described in published literature, software must be made available to editors and reviewers. We strongly encourage code deposition in a community repository (e.g. GitHub). See the Nature Portfolio guidelines for submitting code & software for further information.

Data

Policy information about availability of data

All manuscripts must include a data availability statement. This statement should provide the following information, where applicable:

- Accession codes, unique identifiers, or web links for publicly available datasets
- A description of any restrictions on data availability
- For clinical datasets or third party data, please ensure that the statement adheres to our policy

Data used in this study are collected from the following sources: Population dataset is from WorldPop (https://www.worldpop.org); Global baseline land cover product for 2020 (WorldCover) is from the European Space Agency (https://esa-worldcover.org); The Meta (former Facebook)'s High-Resolution Population Density (HRPD) is from Data for Good platform (https://dataforgood.facebook.com/dfg/tools/high-resolution-population-density-maps); World Settlement Footprint (WSF) maps are from Scientific Data repository (https://www.nature.com/articles/s41597-020-00580-5);Wildfire burned area datasets are from the MODIS data Archive in

Google Earth Engine (https://earthengine.google.com); Global urban area boundaries are from FROM-GLC research group (https://data-starcloud.pcl.ac.cn/); Global industrial and smallholder oil palm map is from Zenodo (https://zenodo.org/record/4473715). Wildland-urban interface data in United States for validation is from the SILVIS lab (http://silvis.forest.wisc.edu/data/wui-change). The 30-m global land-cover product with fine classification system (GLC-FCS) is from Zenodo (https://zenodo.org/record/3986872). The 100-m global human settlement layers (GHSL) is from Joint Research Centre (JRC) of European Commission (https://ghsl.jrc.ec.europa.eu/ghs_buS2023.php). The Global Wildland–Urban Interface datasets for 2020 baseline and 1985-2020 time series have been deposited the following repository: https://datahub.hku.hk/projects/GlobalWUI/191163.

Human research participants

Policy information about studies involving human research participants and Sex and Gender in Research.

Reporting on sex and gender	N.A.
Population characteristics	N.A.
Recruitment	N.A.
Ethics oversight	N.A.

Note that full information on the approval of the study protocol must also be provided in the manuscript.

Field-specific reporting

Please select the one below that is the best fit for your research. If you are not sure, read the appropriate sections before making your selection.

☐ Life sciences ☐ Behavioural & social sciences ☒ Ecological, evolutionary & environmental sciences

For a reference copy of the document with all sections, see nature.com/documents/nr-reporting-summary-flat.pdf

Ecological, evolutionary & environmental sciences study design

All studies must disclose on these points even when the disclosure is negative.

Study description	Intensifying wildfires and human settlement expansion have placed more people and infrastructure at the wildland–urban interface (WUI) areas under risk. Wildfire management and policy response are needed to protect ecosystems and residential communities; however, maps containing spatially explicit information on the distribution of WUI areas are limited to certain countries or local regions, and therefore global WUI patterns and associated wildfire exposure risk remain unclear. Here, we generated the global WUI data layers for 2020 baseline and 1985-2020 time series by incorporating fine-resolution housing and vegetation mapping. We estimated the total global WUI area to be 6.62 million km2. Time-series analysis revealed that global WUI areas experienced a substantial increase of 12.56% between 1985 and 2020. By overlapping 2001-2020 wildfire burned area maps and fine-resolution population dataset, our analysis revealed that globally, 7.07% (12.54%) of WUI areas housing 4.47 million (10.11 million) people are within a 2400-m (4800-m) buffer zone of wildfire threat. Regionally, we found that the United States, Brazil, China, India, and Australia account for the majority of WUI areas, but African countries experience higher wildfire risk. Our quantification of global WUI spatiotemporal patterns and the associated wildfire risk could support improvement of wildfire management.
Research sample	We developed a methodology incorporating fine-resolution housing and vegetation footprint to generate the global wildland-urban interface (WUI) mapping for 2020 baseline and 1985-2020 time series and used the results to elucidate global differences in WUI pattern and associated wildfire risk, specifically at country and state levels.
Sampling strategy	At the GFED regions, country and state levels, we conduct a global analysis.
Data collection	Data used in this study are collected from the following sources: Population dataset is from WorldPop (https://www.worldpop.org); Global baseline land cover product for 2020 (WorldCover) is from the European Space Agency (https://esa-worldcover.org); The Meta (former Facebook)'s High-Resolution Population Density (HRPD) is from Data for Good platform (https://dataforgood.facebook.com/dfg/tools/high-resolution-population-density-maps); World Settlement Footprint (WSF) maps are from Scientific Data repository (https://www.nature.com/articles/s41597-020-00580-5);Wildfire burned area datasets are from the MODIS data Archive in Google Earth Engine (https://earthengine.google.com); Global urban area boundaries are from FROM-GLC research group of Tsinghua University (http://data.ess.tsinghua.edu.cn); Global industrial and smallholder oil palm map is from Zenodo (https://zenodo.org/record/4473715). Wildland-urban interface data in United States for validation is from the SILVIS lab (http://silvis.forest.wisc.edu/data/wui-change). The 30-m global land-cover product with fine classification system (GLC-FCS) is from Zenodo (https://zenodo.org/record/3986872). The 100-m global human settlement layers (GHSL) is from Joint Research Centre (JRC) of European Commission (https://ghsl.jrc.ec.europa.eu/ghs_buS2023.php). Bin Chen and Shengbiao Wu collected and recorded the data.
Timing and spatial scale	We used the results for 2020 to elucidate global difference in wildland-urban interface (WUI) areas and incorporated wildfire burned areas from 2001-2020 to estimate the wildfire risks; and we further used the time-series mapping of global WUI areas to quantify their spatiotemporal changes at 5-year intervals from 1985 to 2020.

Data exclusions	No data was excluded.
Reproducibility	We have followed the framework and guidelines in the 2019 report on reproducibility and replication by the National Science Foundation and the U.S. Department of Education (https://www.nsf.gov/pubs/2019/nsf19022/nsf19022.pdf). For instance, we have provided detailed, transparent, and clear descriptions of the methods (e.g., data sources, methods, analysis procedures) that have led to the findings. We are committed to making all data, methods, code, etc. used in our research available to those interested individuals so that they can be used by others to exactly reproduce our findings.
Randomization	No allocation.
Blinding	No blinding.

Did the study involve field work? ☐ Yes ☒ No

Reporting for specific materials, systems and methods

We require information from authors about some types of materials, experimental systems and methods used in many studies. Here, indicate whether each material, system or method listed is relevant to your study. If you are not sure if a list item applies to your research, read the appropriate section before selecting a response.

Materials & experimental systems

n/a	Involved in the study
☒	☐ Antibodies
☒	☐ Eukaryotic cell lines
☒	☐ Palaeontology and archaeology
☒	☐ Animals and other organisms
☒	☐ Clinical data
☒	☐ Dual use research of concern

Methods

n/a	Involved in the study
☒	☐ ChIP-seq
☒	☐ Flow cytometry
☒	☐ MRI-based neuroimaging